2024 IEEE/RSJ International Conference on Intelligent Robots and Systems (IROS)
October 14-18, 2024. Abu Dhabi, UAE

Dung Beetle Optimizer-based High-precision Localization for Magnetic-Controlled Capsule Robot*

Zijin Zeng, *Student Member*, *IEEE*, Fengwu Wang, Chan Li, *Student Member*, *IEEE*, Menglu Tan, Shengyuan Wang, and Lin Feng*, *Member*, *IEEE*

***Abstract*— As a medical microrobot, magnetic-controlled capsule robots (MCRs) are pivotal in internal diagnostics and therapeutic interventions. Achieving high-precision localization of MCRs is essential for the successful execution of medical procedures. This paper introduces a novel Dung Beetle Optimizer (DBO)-based localization method for MCR, demonstrating high localization accuracy and flexibility in static magnetic field environments and under the control of existing magnetic control systems. With the aid of an FPGA-based parallel measurement system, it can effectively eliminate measurement distortion. The average position and orientation errors could achieve 0.53 mm and 0.60° when performing 600 iterations per computation, and further increasing the number of iterations reduces the errors, which is superior to existing methods. Experimental validations underscore the method's robust performance and compatibility with existing magnetic control systems.**

I. Introduction

Magnetic-controlled capsule robots (MCRs) are micro-robots controlled by external magnetic fields, primarily used in the medical and health fields, especially for non-invasive endoscopic examinations and drug delivery. The development of this technology, supported by the rapid advancement of bioelectronics and biomedical devices [1], offers patients a safe, effective, and comfortable method of examination and treatment, particularly in gastrointestinal inspections [2]-[4]. Magnetic field actuation is deemed the most promising approach for active motion control of capsule robots [5]: the internal permanent magnet allows the robot to execute various movements in an external magnetic field, including translation and rotation. Many scholars have researched the magnetic field control techniques for MCR [6]-[11]. Accurate position and orientation data of the capsule robot are crucial for attaining precise motion control, ensuring stable imaging, and pinpointing lesion locations accurately.

Conventional localization systems based on magnetic fields typically consist of magnetic field sources and sensors. The configuration with the permanent magnet inside the MCR serving as the field source, coupled with multiple external sensors, is preferred over having magnetic sensors inside the MCR to gauge external magnetic fields [12]. This arrangement effectively leverages the internal permanent magnet and simplifies the capsule's design. When using multiple sensors, ensuring the real-time nature of measurements is crucial. Asynchronous measurements can lead to measurement distortion, causing significant errors in high dynamic magnetic fields.

Numerous scholars have explored magnetic localization methods to achieve five degrees of freedom (5-DOF) for objects, encompassing 3D positioning and 2D orientation (yaw and pitch angles). Typically, a set number of magnetic sensors, such as Hall effect sensors [13], are used in conjunction with the physical modeling of the magnet. Various optimization algorithms, including Linear Optimizer [13]-[14], non-linear Optimizer [15], Particle Swarm Optimizer (PSO) [16]-[17], and Simulated Annealing-Particle Swarm Optimizer (SA-PSO) [18]-[19] algorithms, are applied to solve the extensive set of physical equations. The Dung Beetle Optimizer (DBO) [20], as a newly proposed swarm intelligence optimization algorithm, has demonstrated outstanding performance compared to existing optimization techniques, highlighting its potential in solving MCR localization challenges.

This paper presents a novel high-precision localization method for MCR based on DBO that is superior to existing methods. With an FPGA-based parallel magnetic field measurement system, this method effectively eliminates errors caused by measurement distortion. Localization experiments were conducted in the existing MCR control system's static and dynamic magnetic field environments, evaluating position error (PE), orientation error (OE), and computation time (CT) performance under various conditions. This localization method offers good flexibility, allowing for adjustments in computation time and localization accuracy to meet the needs of different application scenarios. Compared to existing technologies, this new method significantly reduces errors, showcasing its exceptional localization capabilities.

II. Localization Method

A. Localization System Model

The localization system for MCR needs to be deployed within the existing MCR magnetic control system based on

*Research supported by Beijing Municipal Fund for Distinguished Young Scholars under Grant No.JQ22022 and National Key R&D Program of China under Grant No.2022YFF1502000.

Zijin Zeng is with School of Mechanical Engineering & Automation, Beihang University, Beijing, China (e-mail: zijin_zeng@163.com).

Fengwu Wang is with School of Mechanical Engineering & Automation, Beihang University, Beijing, China, and BEIGE Institute of Robot & Intelligent Manufacturing, Weifang, Shandong, China (e-mail: zf2107105@buaa.edu.cn).

Chan Li is with School of Mechanical Engineering & Automation, Beihang University, Beijing, China (e-mail: im_lichan@163.com).

Menglu Tan is with School of Mechanical Engineering & Automation, Beihang University, Beijing, China (e-mail: tanmenglu@buaa.edu.cn).

Shengyuan Wang is with School of Mechanical Engineering & Automation, Beihang University, Beijing, China (e-mail: shengyuan1002@buaa.edu.cn).

Lin Feng is with School of Mechanical Engineering & Automation, Beihang University, Beijing, China, and Beijing Advanced Innovation Center for Biomedical Engineering, Beijing, China (corresponding author to provide phone: +86 010-82316603; e-mail: linfeng@buaa.edu.cn).

electromagnetic coils, as illustrated in Figure 1. The system consists of levitation and deflection coils, enabling the MCR's levitation and 5-DOF motion control. This study adopts a localization scheme that utilizes multiple external magnetic sensors to measure the magnetic field generated by the internal permanent magnet of the capsule.

Figure 1. Overview of the existing human-scale magnetic control system for magnetic levitation capsule robot.

Regarding sensor layout, a planar array configuration is chosen and placed as close as possible to the MCR's workspace within the magnetic control system, ensuring effective magnetic field data collection at any position within the MCR's workspace. Compared to a volumetric layout, the advantage of a planar layout lies in its better suitability for the installation requirements of this magnetic control system. For instance, it can be easily integrated into the examination platform located below the patient being examined in the system without interfering with other operations during the process.

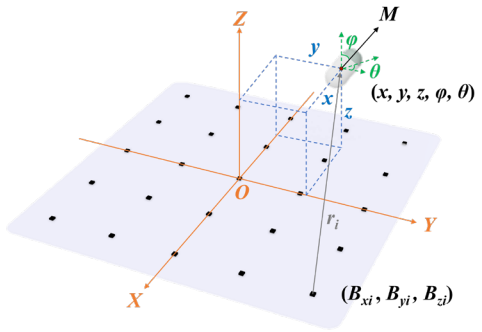

Figure 2. Model of the localization system with 3-axis magnetic sensors in a planar array.

The MCR's internal permanent magnet can be considered a magnetic dipole. The magnetic field detected by each sensor in the spatial arrangement can be calculated. For the sensor layout illustrated in Figure 2, where (x, y, z) represents MCR's position, φ represents the pitch angle, and θ represents the yaw angle. Based on the Biot-Savart Law, the magnetic field distribution of a magnet can be derived [12], leading to the following relationship:

$$\begin{cases} B_{xi} = \dfrac{\mu_r \mu_0 MV}{4\pi}\left\{\dfrac{3(x_i - x)\left[a(x_i - x) + b(y_i - y) + c(z_i - z)\right]}{r_i^5} - \dfrac{a}{r_i^3}\right\} \\ B_{yi} = \dfrac{\mu_r \mu_0 MV}{4\pi}\left\{\dfrac{3(y_i - y)\left[a(x_i - x) + b(y_i - y) + c(z_i - z)\right]}{r_i^5} - \dfrac{b}{r_i^3}\right\} \\ B_{zi} = \dfrac{\mu_r \mu_0 MV}{4\pi}\left\{\dfrac{3(z_i - z)\left[a(x_i - x) + b(y_i - y) + c(z_i - z)\right]}{r_i^5} - \dfrac{c}{r_i^3}\right\} \end{cases} \quad (1)$$

where (B_{xi}, B_{yi}, B_{zi}) represents the magnetic field data measured by the ith sensor located at (x_i, y_i, z_i), while r_i represents the distance from the magnet to the sensor. (a, b, c) represents the unit vector of the magnetic moment. V represents the volume of the magnet, M denotes the magnetization strength, μ_0 indicates the vacuum permeability, and μ_r signifies the relative permeability of the medium.

B. Dung Bettle Optimizer (DBO)-based Localization Method

Resolving equations (1) yields the 5D parameters (x, y, z, φ, θ) crucial for MCR's localization, so an efficient optimization algorithm is vital for minimizing computation time and enhancing localization accuracy. To this end, this research incorporates the DBO to tackle the intricate optimization challenges prevalent in the precise localization of MCR.

The implementation of the DBO algorithm begins by randomly initializing a group of individuals within the optimization region. Throughout the optimization iterations, these individuals engage in specific behaviors according to a set of predefined rules. These behaviors are inspired by the various activities of dung beetles in nature, such as ball-rolling, dancing, foraging, stealing, and reproducing. When applying the DBO algorithm to the localization of MCR, the optimization region is defined as the workspace of the MCR, with each individual representing a hypothetical MCR endowed with a set of randomly assigned 5D parameters. During the optimization iterations, the parameters of all individuals are updated to closely match the anticipated results derived from equations (1). Ultimately, the position where an individual's state best satisfies the requirements of the equations is identified as the global optimum solution, represents the precise location of the MCR.

To better adapt to the application of MCR's localization, appropriate adjustments were made to the original DBO algorithm [20]. The main adjustments include modifying the population size and parameter ranges. The specific implementation process of the novel high-precision localization method for MCR based on DBO is as follows:

The process of implementing the DBO algorithm is shown in Figure 3. The optimization domain is defined as a 120×120×120 mm region, within which 40 individuals are initially dispersed. Each individual possesses 5D localization parameters that are assigned randomly, forming an optimization population. The value of each parameter is considered as the position of the individual in that dimension. For each individual, theoretical three-axis magnetic field measurements are calculated when the MCR's position is aligned with the individual's parameters, based on equations (1). The fitness value F_i, for each individual is determined by comparing these theoretical readings (B_{xi}, B_{yi}, B_{zi}) with the actual sensor readings (B'_{xi}, B'_{yi}, B'_{zi}) using equation (2).

Herein, it is considered that the individual with the smallest fitness is the best, and the one with the largest fitness is the worst. "Global" refers to all individuals, while "local" pertains to individuals within a specific category.

$$F_i = \sum_{i=1}^{25}\left[\left(B_{xi}-B'_{xi}\right)^2+\left(B_{yi}-B'_{yi}\right)^2+\left(B_{zi}-B'_{zi}\right)^2\right] \tag{2}$$

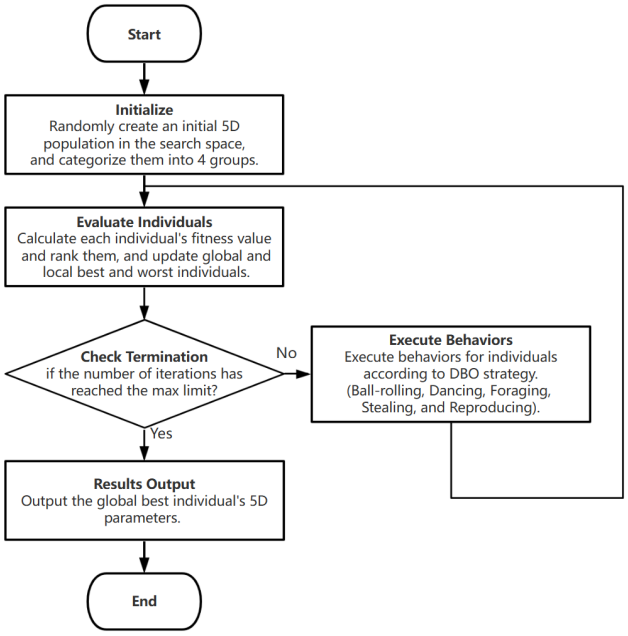

Figure 3. Flowchart for MCR localization using the DBO algorithm.

Following the evaluation of fitness values, the individuals are ranked and divided into four categories according to a 4:4:5:7 ratio, representing rolling, thief, hatching, and small dung beetles, respectively. The rolling dung beetles initiate ball-rolling or dancing behavior, while the other three categories engage in reproducing, stealing, and foraging behaviors as per the DBO algorithm as follows:

Ball-rolling: Individuals perform rolling to move in the direction away from the global worst position as follows:

$$p_i(t+1) = p_i(t) + \alpha \times k \times p_i(t-1) + b \times \left| p_i(t) - p_{gw} \right| \tag{3}$$

where $p_i(t\text{-}1)$, $p_i(t)$, and $p_i(t\text{+}1)$ represent the parameter in the previous, current and next iteration, p_{gw} represents the global worst position, coefficient $k = 0.1$, $a = 1$ or -1, $b = 0.3$.

Dancing: The dancing behavior is a special case of rolling. Individuals perform dancing to prevent them from falling into the local best position as follows:

$$p_i(t+1) = p_i(t) + \tan(\beta) \cdot \left| p_i(t) - p_i(t-1) \right| \tag{4}$$

where deflection angle $\beta \sim [0, \pi]$.

Reproducing: Individuals perform reproducing to find the local best position as follows:

$$\begin{aligned} p_i(t+1) = p_{lb} &+ c_1 \times \left(p_i(t) - \max\left(p_{lb} \times (1-R), Lb_R \right) \right) \\ &+ c_2 \times \left(p_i(t) - \min\left(p_{lb} \times (1+R), Ub_R \right) \right) \end{aligned} \tag{5}$$

where c_1, $c_2 \sim U(0, 1)$. Ub_R and Lb_R represent the bounds of the reproducing area.

Foraging: Individuals performing foraging to find the global best position as follows:

$$\begin{aligned} p_i(t+1) = p_i(t) &+ d_1 \times \left(p_i(t) - \max\left(p_{gb} \times (1-R), Lb_F \right) \right) \\ &+ d_2 \times \left(p_i(t) - \min\left(p_{gb} \times (1+R), Ub_F \right) \right) \end{aligned} \tag{6}$$

where coefficient d_1, $d_2 \sim U(0, 1)$. Ub_F and Lb_F represent the bounds of the foraging area.

Stealing: Individual stealing is a search between global and local best position. The update process involved is as follows:

$$p_i(t+1) = p_{gb} + S \times g \times \left(\left| p_i(t) - p_{lb} \right| + \left| p_i(t) - p_{gb} \right| \right) \tag{7}$$

where coefficient $S = 0.5$, and $g \sim N(5, 1)$.

After executing these behaviors, fitness values are re-evaluated and ranked. If the global best position improves, it is updated, and so do the global worst position and local best position. This iterative process continues until reaching the predetermined number of iterations, concluding a cycle of the localization computation. After the final iteration, the global best position will be output as the ultimate localization result.

C. Magnetic Field Decouple

The localization of MCR relies solely on the magnetic field generated by its internal permanent magnet. However, when operating under the magnetic control system, the sensors within the measurement system will additionally detect the magnetic field generated by the control system, due to the principle of magnetic field superposition. Consequently, separating these two magnetic field components through an appropriate method is essential for achieving accurate localization.

In this study, the magnetic field is generated by electromagnetic coils equipped with precision current sensors. The localization system is installed at designated fixed positions, and magnetic sensors measure the field produced by each coil under varying current conditions. Based on the readings from these sensors, a magnetic field-current model for the magnetic control system can be constructed. When the magnetic control system operates, the magnetic field generated by the coils can be calculated in real time based on the current as follows:

$$\begin{bmatrix} B_{C1x} & B_{C1y} & B_{C1z} \\ B_{C2x} & B_{C2y} & B_{C2z} \\ \vdots & \vdots & \vdots \\ B_{Ci1x} & B_{Ciy} & B_{Ciz} \end{bmatrix} = \begin{bmatrix} B_{1x} & B_{1y} & B_{1z} \\ B_{2x} & B_{2y} & B_{2z} \\ \vdots & \vdots & \vdots \\ B_{ix} & B_{iy} & B_{iz} \end{bmatrix} - \begin{bmatrix} I_1 \\ I_2 \\ \vdots \\ I_n \end{bmatrix} T \tag{8}$$

where B_{C1}, B_{C2}, … B_{Ci} denote the magnetic field components produced by the internal permanent magnets. B_1, B_2, ... B_i correspond to the magnetic field measurements recorded by each sensor. I_1, I_2, … I_n represent the currents flowing through the coils, while T is the transformation matrix that maps these currents to the magnetic fields generated by the coils. This decoupling of the two magnetic field components allows the

isolation of the pure magnetic field contribution from the MCR's internal magnets, enabling accurate localization.

III. Experiments and Results

A. Localization System Setup

Reading measurements from an extensive sensor array, utilizing a conventional single-threaded microcontroller for communications is efficient but faces limitations. However, for certain applications using I^2C, some sensors have non-customizable device addresses, leading to address conflicts. In these cases, an I^2C bus multiplexer is required. It's noteworthy that this multiplexer communication introduces additional I^2C write operations, extending the sensor reading time. Consequently, sensors are queued, and the microcontroller sequentially interacts with each through the multiplexer, resembling a rolling shutter mechanism where sensor readings aren't simultaneous, leading to measurement distortions. Such a setup poses significant challenges in environments with rapidly changing and complex magnetic fields. To address this, this research employs an FPGA to develop a multi-channel, real-time, magnetic field parallel measurement system, enabling simultaneous readings from all sensors to significantly reduce total measurement time and mitigate distortion. Taking the reading of 25 sensors as an example, Table 1 illustrates the difference in time between sequential reading and parallel reading.

TABLE I. Comparison of Sequential and Parallel Reading of 25 Sensors.

Strategy	Multiplexer Required	Multiplexer Communication Time	Single Sensor Read Time	Total Sensors Read Time
Sequential	Yes	20 us	275 us	7,375 us
Parallel	No	0	275 us	275 us

The MCR used in the experiment contains an axially magnetized N52 NdFeB magnet sized Ø10×5 mm at its center of gravity. As Figure 4 shows, the real-time magnetic field parallel measurement system incorporates a 5×5 sensor array and an FPGA. The sensors, positioned 30 mm apart within the array, are Memsic MMC5603NJ three-axis anisotropic magnetoresistive (AMR) sensors, capable of measuring at frequencies up to 1000 Hz via I^2C interface. The FPGA employed is the Xilinx XC7Z020CLG484. All data processing during the experiment is carried out in MATLAB deployed on a Windows 10 platform. Localization experiments were conducted in environments both without and with the intervention of a magnetic control system.

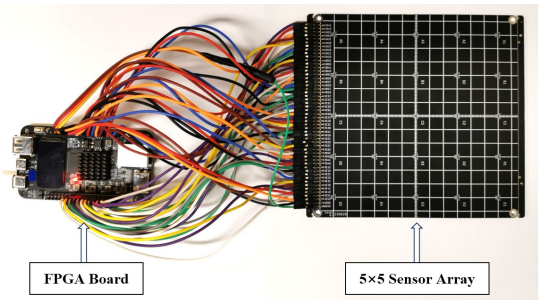

Figure 4. 25-channel real-time magnetic field parallel measurement system.

B. Localization Experiments and Analysis

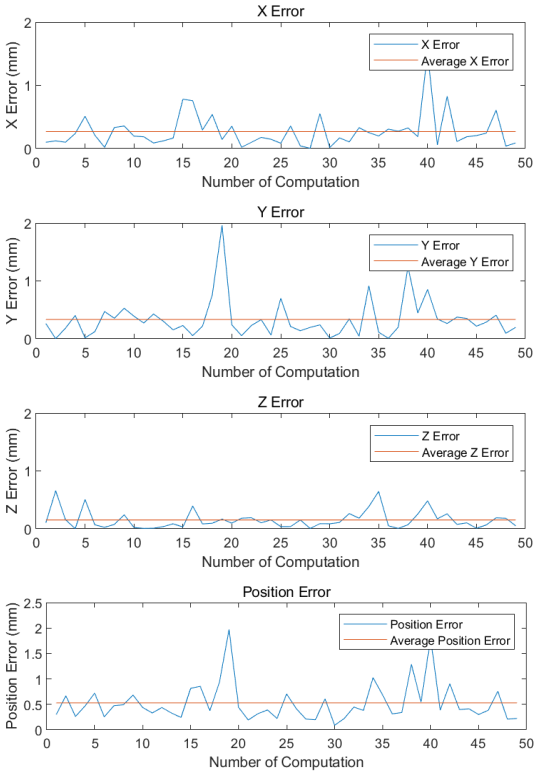

Figure 5. Position error when performing 600 iterations per computation.

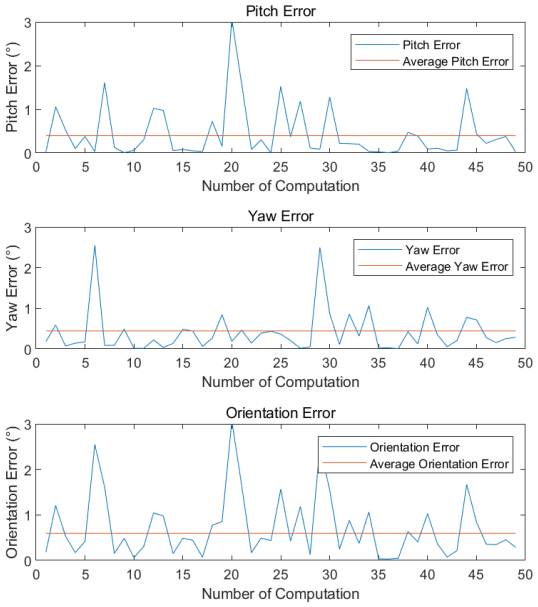

Figure 6. Orientation error when performing 600 iterations per computation.

When conducting localization experiments in an environment without magnetic control system intervention, the MCR is fixed in the workspace with an 6-axis robotic arm, maintaining pre-set known 5D parameters. Figures 5 and 6 display the PE and OE, respectively, for 50 consecutive computations using the DBO algorithm, with each computation comprising 600 iterations. The results indicate that the average PEs along the *x*, *y*, and *z* axes are 0.27 mm, 0.33 mm, and 0.15 mm, respectively, leading to an overall

average PE of 0.53 mm. Additionally, the pitch and yaw angles exhibit average errors of 0.44° and 0.40°, respectively, resulting in a combined average OE of 0.60°. This performance showcases the system's exceptional localization precision, marked by minimal discrepancies in both positioning and orientation.

Localization performance is gauged by three pivotal metrics: PE, OE, and CT, and the number of iterations significantly impacts them to delineate this correlation, experiments across varied numbers of iterations were conducted. Figures 7 and 8 display how these metrics vary with the number of iterations. As the iterations increase, a noticeable trend in error reduction is observed, highlighting the effectiveness of the iterative process in minimizing errors. Nonetheless, this accuracy enhancement incurs an uptick in CT, diminishing the frequency of localization updates. At 50 iterations, the CT is 280 ms, yielding a PE of 2.70 mm and an OE of 2.31°. Elevating iterations to 1000 prolongs the CT to 1400 ms but lowers the PE to 0.30 mm and OE to 0.48°.

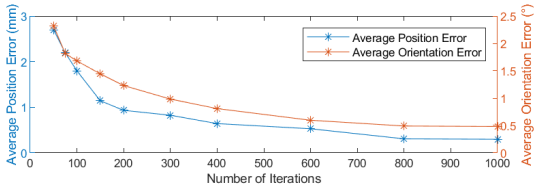

Figure 7. Relationship between the number of iterations and errors.

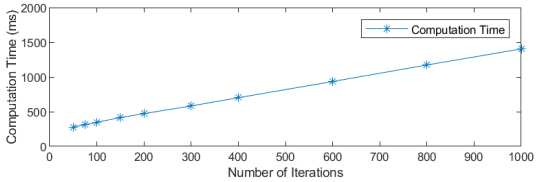

Figure 8. Relationship between the number of iterations and computation time.

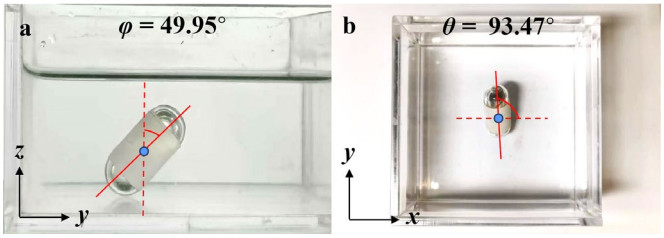

Figure 9. Illustration of MCR maintaining a specific pose controlled by the magnetic control system. (a) pitch angle $\varphi = 49.95°$. (b) yaw angle $\theta = 93.47°$.

In engineering contexts, striking a balance between errors and CT is crucial to optimize the trade-off between them. The selection of an appropriate number of iterations is determined by the specific needs of the application. For example, magnetic levitation control of the MCR requires higher control frequencies, thus necessitating shorter CT. Conversely, applications centered around pose estimation can afford longer CT. Moreover, the processing capability of the upper computer plays a significant role in affecting the CT, suggesting that performance can differ across platforms. Utilizing a more powerful computing system can markedly reduce CT.

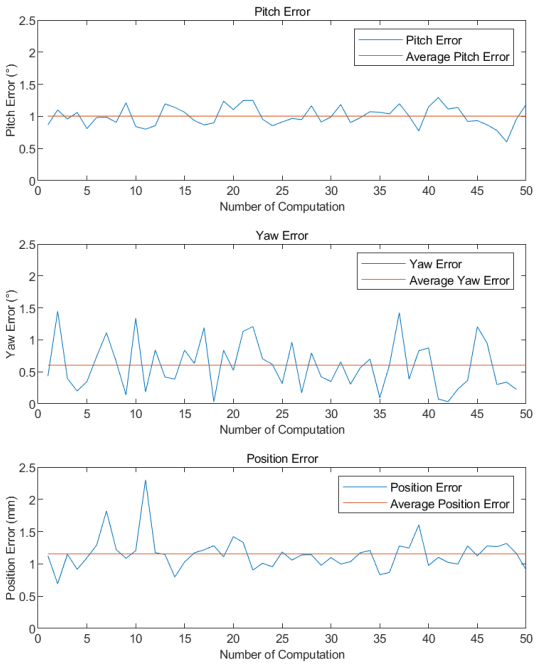

Figure 10. The errors of the localization system when operating concurrently with the magnetic control system.

The MCR operates under the magnetic control system, necessitating simultaneous functioning with the localization system. Through the magnetic field decoupling method described earlier, the control system's magnetic field distribution under various current conditions is pre-measured, and a magnetic field-current model for the system is constructed. This allows for localization to occur simultaneously with the operation of the magnetic control system. Figure 9 shows the MCR maintaining a certain posture under magnetic control, with the 5D parameters determined through a camera system and image analysis. Figure 10 shows localization errors with 600 iterations per calculation, demonstrating robust performance even with concurrent magnetic control. The average pitch angle error is 1.00°, the average yaw angle error is 0.60°, the average OE is 1.17° and the average PE is 1.15 mm.

It is noted that errors slightly increase under magnetic control compared to a stable external environment. This discrepancy is due to the magnetic field-current model's deviation from actual conditions, suggesting that more precise and accurate modeling could further enhance accuracy. Spikes observed in the results, regardless of the presence of a magnetic control system, may be attributed to noise encountered during the measurement and electromagnetic interference from the environment, leading to results being trapped in local optima. Therefore, the application of effective real-time filtering algorithms is also necessary to minimize their impact.

Table 2 presents a comparison of the DBO localization algorithm with several existing methods in terms of PE, OE, and CT. The DBO algorithm outperforms the existing algorithms, showcasing its robust localization capabilities.

TABLE II. LOCALIZATION PERFORMANCE COMPARISON OF DIFFERENT METHODS.

Research	Method	CT	PE	OE	Note
[13]	Linear Optimizer	137 ms	5.6 mm	4.26%	Experimental result
[14]	Linear Optimizer	100-200 ms	5.6 mm	4.5°	Experimental result
[15]	Linear/Non-linear Optimizer	N/A	3.72 mm (linear) / 2.07 mm (non-linear)	1.86° (linear) / 1.61° (non-linear)	Experimental result
[16]	PSO	170 ms / 630 ms (improved)	3.90 mm / 0.59 mm (improved)	5.06° / 0.66° (improved)	Noise-free simulation result
[17]	PSO	830 s	0.003 mm	0.036°	Noise-free simulation result
[18]	SA-PSO	N/A	1.64 mm (static environment) / 1.61 mm (magnetic control)	1.08° (static environment) / 1.5° (magnetic control)	Experimental result
This Research	DBO	840 ms	0.53 mm (static environment) / 1.15 mm (magnetic control)	0.60° (static environment) / 1.17° (magnetic control)	Experimental result, localization performance adjustable as needed

IV. CONCLUSION

This study introduces a novel, high-precision localization method for MCR, utilizing the DBO algorithm and an FPGA-based parallel measurement system to surpass traditional methods. By mitigating measurement distortions, this approach ensures superior accuracy in both static and dynamic magnetic fields of the MCR control system. Comprehensive testing showed improved performance in PE, OE, and CT that are adjustable as needed, offering notable flexibility for diverse applications. When each calculation performs 600 iterations, the PE achieves 0.53mm and the OE achieves 0.60° in a stable magnetic field. Under magnetic control, the PE can reach 1.15mm and the OE can reach 1.17°.

This method demonstrates its potential for future technologies such as magnetic levitation control, guidewire robot navigation, and AR/VR applications. Additionally, combining bio-inspired actuator technology [21] with robotic localization systems warrants further exploration. The use of emerging wearable flexible sensor technology [22] will help to further enhance the accuracy and flexibility of these systems.

REFERENCES

[1] N. Zhou and L. Ma, "Smart bioelectronics and biomedical devices," *Bio-Design and Manufacturing*, vol. 5, no. 1, pp. 1–5, Jan. 2022.

[2] V. K. Sharma, "The future is wireless: advances in wireless diagnostic and therapeutic technologies in gastroenterology," *Gastroenterology*, vol. 137, no. 2, pp. 434–439, Aug. 2009.

[3] R. A. Enns *et al*., "Clinical Practice Guidelines for the Use of Video Capsule Endoscopy," *Gastroenterology*, vol. 152, no. 3, pp. 497–514, Feb. 2017.

[4] A. Wang *et al.*, "Wireless capsule endoscopy," *Gastrointestinal Endoscopy*, vol. 78, no. 6, pp. 805–815, Dec. 2013.

[5] W. Chen, J. Sui, and C. Wang, "Magnetically Actuated Capsule Robots: A Review," *IEEE Access*, vol. 10, pp. 88398–88420, 2022.

[6] Z. Liao *et al.*, "Accuracy of Magnetically Controlled Capsule Endoscopy, Compared With Conventional Gastroscopy, in Detection of Gastric Diseases," *Clinical Gastroenterology and Hepatology*, vol. 14, no. 9, pp. 1266–1273.e1, Sep. 2016.

[7] H. Lai *et al.*, "Standing-type magnetically guided capsule endoscopy versus gastroscopy for gastric examination: multicenter blinded comparative trial," *Digestive Endoscopy*, vol. 32, no. 4, pp. 557–564, Oct. 2019.

[8] A. W. Mahoney and J. J. Abbott, "5-DOF Manipulation of an Untethered Magnetic Device in Fluid using a Single Permanent Magnet," *CiteSeer X (The Pennsylvania State University)*, Jul. 2014.

[9] J. Wei, L. Song, X. Wang, J. Zhao, and L. Feng, "5 DOF Capsule Endoscopy with Wi-Fi based Video Transmission Module," in *2021 WRC Symposium on Advanced Robotics and Automation (WRC SARA)*, pp. 134–139, Sep. 2021.

[10] L. Song *et al.*, "The Design of 3-D Space Electromagnetic Control System for High-Precision and Fast-Response Control of Capsule Robot with 5-DOF," in *2019 International Conference on Intelligent Robotics and Applications*, pp. 202–212, Jan. 2019.

[11] O. Tovmachenko, L. Feng, A. M. Mousa, Z. Ullah, and M. A. Masoud, "A Capsule-Type Device for Soft Tissue Cutting Using a Threadless Ballscrew Actuator," in *2019 International Conference on Manipulation, Automation and Robotics at Small Scales (MARSS)*, pp. 1–6, Jul. 2019.

[12] F. Bianchi *et al.*, "Localization strategies for robotic endoscopic capsules: a review," *Expert Review of Medical Devices*, vol. 16, no. 5, pp. 381–403, May 2019.

[13] C. Hu, Max Q.-H. Meng, and M. Mandal, "Efficient magnetic localization and orientation technique for capsule endoscopy," in *2005 IEEE/RSJ International Conference on Intelligent Robots and Systems*, pp. 628–633, Jan. 2005.

[14] X. Wang, Max Q.-H. Meng, and C. Hu, "A Localization Method Using 3-axis Magnetoresistive Sensors for Tracking of Capsule Endoscope," in *2006 International Conference of the IEEE Engineering in Medicine and Biology Society*, pp. 2522–2525, Aug. 2006.

[15] C. Hu, W. Yang, D. Chen, Max Q.-H. Meng, and H. Dai, "An improved magnetic localization and orientation algorithm for wireless capsule endoscope," in *2008 30th Annual International Conference of the IEEE Engineering in Medicine and Biology Society*, pp. 2055–2058. Aug. 2008.

[16] W. Yang, C. Hu, Max Q.-H. Meng, S. Song, and H. Dai, "A Six-Dimensional Magnetic Localization Algorithm for a Rectangular Magnet Objective Based on a Particle Swarm Optimizer," *IEEE Transactions on Magnetics*, vol. 45, no. 8, pp. 3092–3099, Aug. 2009.

[17] S. Song *et al.*, "6-D Magnetic Localization and Orientation Method for an Annular Magnet Based on a Closed-Form Analytical Model," *IEEE Transactions on Magnetics*, vol. 50, no. 9, pp. 1–11, Sep. 2014.

[18] J. Yang, J. Wei, F. Wang, L. Song, J. Zhao, and L. Feng, "A Localization Method for the Magnetic Levitation Capsule Robot," in *2022 WRC Symposium on Advanced Robotics and Automation (WRC SARA)*, pp. 152–159, Aug. 2022.

[19] Z. Zeng, F. Wang, J. Zhao, C. Wang, C. Li and L. Feng, "The Control System for 5-DOF Magnetic Levitation Capsule Robot," in *2023 WRC Symposium on Advanced Robotics and Automation (WRC SARA)*, pp. 174–179, Aug. 2023.

[20] J. Xue and B. Shen, "Dung beetle optimizer: a new meta-heuristic algorithm for global optimization," *The Journal of Supercomputing*, Nov. 2022.

[21] Y. Wang, C. Liu, L. Ren, and L. Ren, "Bioinspired soft actuators with highly ordered skeletal muscle structures," *Bio-Design and Manufacturing*, vol. 5, no. 1, pp. 174–188, Jul. 2021.

[22] W. Heng, G. Yang, W. S. Kim, and K. Xu, "Emerging wearable flexible sensors for sweat analysis," *Bio-Design and Manufacturing*, vol. 5, no. 1, pp. 64–84, Dec. 2021.